

CERN-TH/97-96
JYFL 6/97
5 May 1997
nucl-th/9705015

HYDRODYNAMICS OF NUCLEAR COLLISIONS WITH INITIAL CONDITIONS FROM PERTURBATIVE QCD

K.J.Eskola^{a,b,1}, K. Kajantie^{a,b,2} and P.V. Ruuskanen^{c,3}

^a *CERN/TH, CH-1211 Geneve 23, Switzerland*

^b *Department of Physics, P.O.Box 9, 00014 University of Helsinki, Finland*

^c *Department of Physics, University of Jyväskylä, P.O.Box 35, 40351 Jyväskylä,
Finland*

Abstract

We compute the longitudinal hydrodynamic flow in ultrarelativistic heavy ion collisions at $\sqrt{s} = 5500$ GeV by using boost non-invariant initial conditions following from perturbative QCD. The transfer of entropy and energy from the central region to larger rapidities caused by boost non-invariance is determined and the associated decrease in the lifetime of the system is estimated.

¹kari.eskola@cern.ch

²keijo.kajantie@cern.ch

³ruuskanen@jyfl.jyu.fi

1 Introduction

One simple scenario for treating the behaviour of QCD matter formed in the central region (nearly at rest in the center of mass frame) in ultrarelativistic heavy ion collisions is to neglect transverse motion and baryon number, to assume that the initial conditions for longitudinal motion are longitudinally boost invariant and to assume that the matter expands isentropically as an ideal fluid. One then obtains the Bjorken similarity flow [1]. The purpose of this study is to take the initial conditions essentially as given by perturbative QCD [2]-[5]. These have two characteristics. Firstly, they are boost non-invariant, there is no rapidity plateau but a wide gaussian-like rapidity distribution. Secondly, due to the remarkable small- x increase of the nucleon structure functions observed at HERA [6] the initial energy densities are quite large, at LHC energies of $\sqrt{s}= 5.5$ TeV almost 1000 GeV/fm^3 . This leads to rather long hydrodynamical evolution times (≈ 100 times initial thermalisation time) and allows a boost non-invariant flow to develop. In the following we shall, in particular, study the additional longitudinal flow caused by the maxima of the initial entropy and energy densities at $y = 0$ and the associated transfer of entropy and energy from the $y = 0$ region to larger rapidities.

We limit this study to LHC energies for the following two reasons. Firstly, we want to study longitudinal 1+1d hydrodynamical effects and at LHC, due to the very large initial temperatures, this period lasts by far the longest. Also, during all this period the matter remains in the high T plasma phase. All the complications associated with the phase transition and the hadronic phase arise together with the need to go over to 1+3d expansion [7]-[8]. Within the 1+1d approximation these late-time features have been studied in, say, [9]. Secondly, at LHC energies the perturbative computation of the initial conditions is more reliable. At RHIC energies of $\sqrt{s}= 200$ GeV there is still a sizable soft component present, which makes the buildup of the initial energy density slower and would require separate modeling [10]. This is even more so at the SPS energies of $\sqrt{s}= 20$ GeV, where boost non-invariant initial conditions are modelled by using rapidity distributions of final state particles [11] or by forcing the flow to be boost invariant [12].

We also emphasize that the main aim is to study the evolution of the flow under a set of approximations which will need corrections when applied to the physical situation. These include full thermalisation and validity of given initial conditions at very large rapidities. Also fluctuations in the initial conditions [13] and their variation with transverse coordinate will have to be taken into account.

2 The equations

For the ultrarelativistic 1+1-dimensional similarity flow it is convenient to replace $x^\mu = (t, x)$ by the proper time τ and the space-time rapidity η :

$$\tau = \sqrt{t^2 - x^2}, \quad \eta = \frac{1}{2} \log \frac{t+x}{t-x}, \quad (1)$$

$$t = \tau \cosh \eta, \quad x = \tau \sinh \eta. \quad (2)$$

The variable

$$\hat{t} = \log(\tau/\tau_i) \quad (3)$$

also naturally appears. The general equation of state with one conserved quantum number is

$$p = p(T, \mu), \quad (4)$$

$$s = \frac{\partial p}{\partial T}, \quad n_q - n_{\bar{q}} \equiv n = 3n_B = \frac{\partial p}{\partial \mu}, \quad \epsilon = Ts - p + \mu n. \quad (5)$$

The aim now is to determine, for given initial conditions, the pressure $p(t, x)$ and the flow $v(t, x) \equiv \tanh \Theta(t, x)$ from the hydrodynamic equations

$$\partial_\mu T^{\mu\nu} = 0, \quad \nu = 0, 1, \quad \partial_\mu J_B^\mu = 0, \quad (6)$$

where

$$T^{\mu\nu} = (\epsilon + p)u^\mu u^\nu - pg^{\mu\nu}, \quad J_B^\mu = n_B u^\mu, \quad (7)$$

$$u^\mu = (\gamma, \gamma v) = (\cosh \Theta, \sinh \Theta). \quad (8)$$

From eqs. (7) and (5) it follows that $u_\nu \partial_\mu T^{\mu\nu} - 3\mu \partial_\mu J_B^\mu = T \partial_\mu s^\mu$, where $s^\mu = su^\mu$ is the entropy current, so that these equations imply entropy conservation:

$$\partial_\mu s^\mu = 0, \quad s^\mu = su^\mu. \quad (9)$$

To express eqs. (6) in component form it is convenient to take their components parallel ($u_\nu \partial_\mu T^{\mu\nu} = 0$) and orthogonal ($(g_{\alpha\nu} - u_\alpha u_\nu) \partial_\mu T^{\mu\nu} = 0$, $\alpha = 0, 1$) to u_μ . The equations to be solved then become [14]

$$(\partial_{\hat{t}} + \bar{v} \partial_\eta) \epsilon + (\epsilon + p)(\bar{v} \partial_{\hat{t}} + \partial_\eta) \Theta = 0, \quad (10)$$

$$(\bar{v} \partial_{\hat{t}} + \partial_\eta) p + (\epsilon + p)(\partial_{\hat{t}} + \bar{v} \partial_\eta) \Theta = 0, \quad (11)$$

$$(\partial_{\hat{t}} + \bar{v} \partial_\eta) n_B + n_B (\bar{v} \partial_{\hat{t}} + \partial_\eta) \Theta = 0, \quad (12)$$

where

$$\bar{v}(\tau, \eta) = \tanh[\Theta(\tau, \eta) - \eta], \quad (13)$$

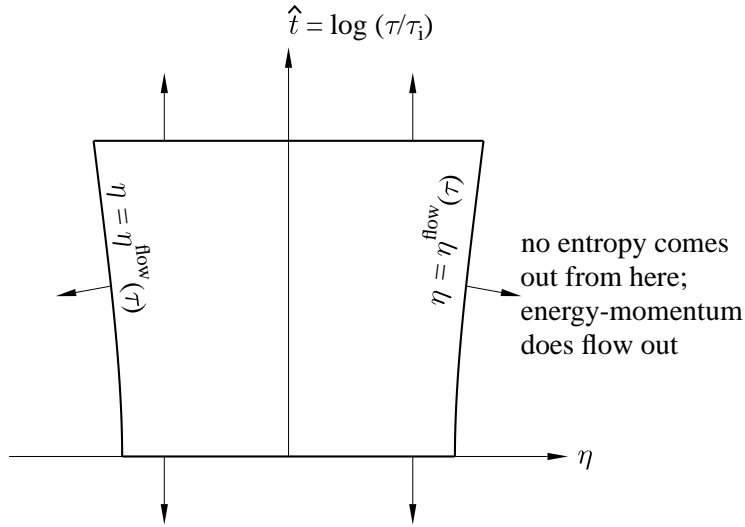


Figure 1: Section of space-time between two flow lines (eq. (15)) and two lines of constant proper time.

with given initial conditions $T = T(\tau_i, \eta)$, $\mu = \mu(\tau_i, \eta)$.

To correctly interpret the numerical results it is useful to have a concrete picture of the role played by the conservation laws in the flow. This is obtained by writing for any conserved vector V^μ

$$0 = \int d^2x \partial_\mu V^\mu = \int_C d\sigma_\mu V^\mu, \quad (14)$$

with $dx^\mu = (dt, dx)$ and $d\sigma^\mu = (dx, dt)$ and choosing the path as shown in Fig. 1. Here the horizontal lines are two lines of constant τ while the vertical lines are chosen as flow lines $\eta = \eta^{\text{flow}}(\tau)$, defined as the solutions of

$$\frac{dx(t)}{dt} = v(x(t), t) \Rightarrow \tau \frac{d\eta}{d\tau} = \bar{v}(\tau, \eta(\tau)) = \tanh[\Theta(\tau, \eta) - \eta]. \quad (15)$$

Computing the line integral (14) over various portions of the path in Fig. 1 gives the fluxes of V^μ through these portions; their total sum has to vanish.

Take first $V^\mu = s^\mu$. Converting the line integral in eq. (14) to the variables τ, η using $u^\mu = (\cosh \Theta, \sinh \Theta)$ one finds that

$$\int_C d\sigma_\mu s^\mu = \int_C \tau \cosh(\Theta - \eta) s [d\eta - \tanh(\Theta - \eta) d\tau / \tau]. \quad (16)$$

Thus the entropy flux through a flow line (15) is zero ($d\sigma_\mu u^\mu = 0$ is an equivalent definition of a flow line) while the flow through a line $\tau = \text{constant}$ is

$$S(\tau, \eta_1 < \eta < \eta_2) = \int_{\eta_1}^{\eta_2} d\eta \tau s(\tau, \eta) \cosh[\Theta(\tau, \eta) - \eta]. \quad (17)$$

Varying now τ and letting $\eta_1(\tau), \eta_2(\tau)$ follow flow lines, eq. (14) implies that the integral (17), the total entropy measured between two flow lines at a fixed proper time, is constant, independent of τ . A similar equation holds for J_B^μ .

We may also apply eq. (14) to the energy and momentum fluxes $T^{0\mu}$ and $T^{1\mu}$. Since they are not proportional to u^μ , the result becomes more complicated. A similar computation gives that the flux through a flow line is:

$$F_E(\tau_1 < \tau < \tau_2) = - \int_{\tau_1}^{\tau_2} d\tau \frac{p \sinh \Theta}{\cosh[\Theta - \eta^{\text{flow}}(\tau)]}, \quad (18)$$

$$F_P(\tau_1 < \tau < \tau_2) = - \int_{\tau_1}^{\tau_2} d\tau \frac{p \cosh \Theta}{\cosh[\Theta - \eta^{\text{flow}}(\tau)]}, \quad (19)$$

where the arguments of Θ, p are $\tau, \eta^{\text{flow}}(\tau)$. Further, the energy and momentum fluxes through a segment $\tau = \text{constant}$ are:

$$E(\tau, \eta_1 < \eta < \eta_2) = \int_{\eta_1}^{\eta_2} d\eta \tau [\epsilon \cosh \Theta \cosh(\Theta - \eta) + p \sinh \Theta \sinh(\Theta - \eta)], \quad (20)$$

$$P(\tau, \eta_1 < \eta < \eta_2) = \int_{\eta_1}^{\eta_2} d\eta \tau [\epsilon \sinh \Theta \cosh(\Theta - \eta) + p \cosh \Theta \sinh(\Theta - \eta)], \quad (21)$$

where the arguments of ϵ, p, Θ are τ, η . Referring to Fig. 1, the total sum of two contributions of type (18) and of two contributions of type (20) has to vanish for $T^{0\mu}$; similarly for $T^{1\mu}$. This implies that the energy (eq. (20)) or momentum (eq. (21)) between two flow lines is not constant but changes due to energy or momentum flow across the flow line: work done against expansion.

Note the different flow-dependent factors in (17) and (20): the total energy E contains an additional boost factor $\cosh \Theta$ not present for S .

To have a still simpler view of the conservation laws, assume a similarity flow, $\Theta(\tau, \eta) = \eta$ or $v(t, x) = x/t$ and an equation of state $p = p(\epsilon)$. Then $\bar{v} = 0$ and from eq. (15) the flow lines are $\eta = \text{constant}$ and we take them to be $\pm\eta_0$. For this very special flow the equations of motion (6) become

$$\tau \partial_\tau \epsilon + \epsilon + p = 0, \quad (22)$$

$$\partial_\eta p = 0, \quad (23)$$

$$\tau \partial_\tau n + n = 0, \quad (24)$$

$$\tau \partial_\tau s + s = 0, \quad (25)$$

(the last follows from the first and third and $\epsilon + p = Ts + \mu n$) and further imply that

$$p = p(\tau), \quad \epsilon = \epsilon(\tau), \quad s = s(\tau, \eta) = \frac{\tau_i}{\tau} s(\tau_i, \eta), \quad n = n(\tau, \eta) = \frac{\tau_i}{\tau} n(\tau_i, \eta), \quad (26)$$

i.e. p, ϵ depend on τ only while s, n can depend also on η in such a way that $Ts + \mu n$ depends only on τ . The conservation laws of $s^\mu, T^{0\mu}$ then simplify to

$$\int_{-\eta_0}^{\eta_0} d\eta [\tau_1 s(\tau_1, \eta) - \tau_2 s(\tau_2, \eta)] = 0, \quad (27)$$

$$\int_{-\eta_0}^{\eta_0} d\eta \cosh \eta [\tau_1 \epsilon(\tau_1) - \tau_2 \epsilon(\tau_2)] = 2 \int_{\tau_1}^{\tau_2} d\tau p(\tau) \sinh \eta_0; \quad (28)$$

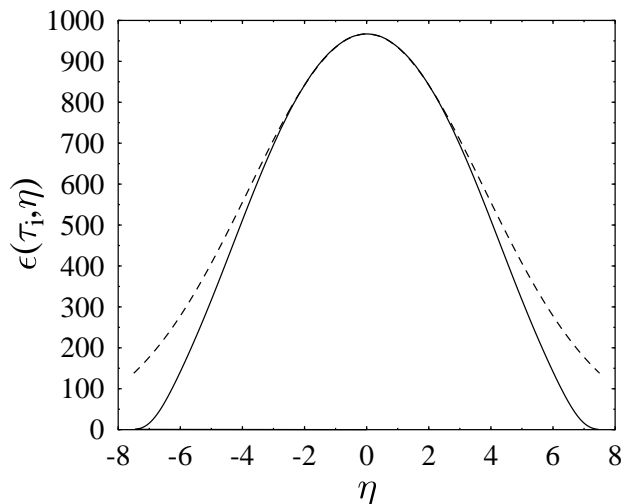


Figure 2: The initial condition for $\epsilon(\tau_i, \eta)$ for $\sqrt{s} = 5500$ GeV. The dashed curve is the gaussian fit, eq. (31), with $\sigma = 3.8$.

similar ones hold for $J_B^\mu, T^{1\mu}$. Eq.(27) is clearly an integrated form of eq.(25). In eq.(28) the η dependent parts factor and match on two sides of the equation. The τ dependent part explicitly shows how the change in $\epsilon(\tau)\tau$ is related to $pdV \sim pd\tau$.

A further step of simplification would be to assume a massless equation of state, $p = \epsilon/3 = aT^4 + b\mu^2T^2 + c\mu^4$, $a, b, c = \text{constants}$. Then a solution with a similarity flow would be

$$T(\tau, \eta) = \left(\frac{\tau_i}{\tau}\right)^{1/3} T(\tau_i, \eta), \quad \mu(\tau, \eta) = \left(\frac{\tau_i}{\tau}\right)^{1/3} \mu(\tau_i, \eta), \quad p(\tau) = \left(\frac{\tau_i}{\tau}\right)^{4/3} p(\tau_i), \quad (29)$$

where $T(\tau_i, \eta), \mu(\tau_i, \eta)$ are so constrained that $p(\tau_i)$ is independent of η . This is the standard Bjorken flow [1] generalised by the inclusion of baryon number. Putting $\mu = 0$ finally gives the Bjorken flow.

3 Initial conditions

One expects the initial net baryon number to very small near $y = 0$; in [5] the net baryon number-to-entropy ratio, B/S was computed to be about 1/5000. Hence, we shall put the chemical potential $\mu = 0$. Further, we are interested in the evolution of the system in the plasma phase, $T = T_c \dots 7T_c$ and choose the equation of state to be $p = p(T) = \epsilon/3 = aT^4$, $a = \text{constant}$, $s = p'(T) = (\epsilon + p)/T$. According to lattice data for pure SU(3) [15] the validity of $p = \epsilon/3$ improves with increasing T so that the error is 20% at $T = 2T_c$ and 10% at $T = 3T_c$.

The initial conditions have to specify $\epsilon(\tau_i, \eta)$ and $\Theta(\tau_i, \eta)$. For the initial flow we shall simply take a similarity flow, $\Theta(\tau_i, \eta) = \eta$, in order to study how boost non-invariance affects it. The initial conditions for the energy density are computed by extending the

calculations of [4]-[5] to all rapidities. The initial energy per unit rapidity in the local rest frame equals the transverse energy of produced minijets computed from

$$\epsilon(\tau_i, \eta) = \frac{dE}{d\eta} \frac{1}{V} \approx T_{AA}(\mathbf{b} = 0) \int_{p_0}^{\infty} dp_T p_T \frac{d\sigma^{NN}}{dp_T dy} \cdot \frac{1}{V}, \quad (30)$$

where the nuclear overlap function is $T_{AA}(0) \approx A^2/(\pi R_A^2) \approx 32/\text{mb}$ for Pb+Pb, the volume per unit rapidity is $V = \tau_i \pi R_A^2$, $1/\tau_i = p_0 = 2$ GeV and the inclusive gluon jet production cross section in NN collisions is computed in [5]. The results for $\tau_i = 0.1$ fm are shown in fig. 2 for LHC energies, $\sqrt{s} = 5500$ GeV, together with a gaussian fit to the central region

$$\epsilon(\tau_i, \eta) = \epsilon_0 \exp[-\eta^2/(2\sigma^2)], \quad (31)$$

with $\sigma = 3.8$. The distribution is seen to be quite broad. In this sense boost non-invariance is quite mild in the central region, even though evidently the initial condition has to drop faster than a gaussian at the ends of phase space. As a side remark, at RHIC energy $\sqrt{s} = 200$ GeV the width parameter is $\sigma = 2.05$.

In the initial values of ϵ_i in fig. 2 only gluons with $p_T \geq 2$ GeV are included. The value 2 GeV corresponds to the saturation limit at LHC energies [5] and the resulting ϵ_i can be expected to be a good estimate for the total energy density. At RHIC energies the saturation limit is lower, only about 1 GeV. This is so low a scale that perturbation theory becomes unreliable. One could also try to keep the minimum p_T of partons included in the computation at the fixed value of 2 GeV; at RHIC energies one then should also include a sizable (about 50%) soft component if one wants to model the entire event. Modeling the soft component is certainly possible but we wish to avoid this phenomenological analysis [10] in the present work.

According to eq.(20) the total initial energy carried by the flow in the interval $-\eta_0 < \eta < \eta_0$ is, estimating the transverse area to be πR_A^2 ,

$$E_{\text{tot}}(\tau_i) = \pi R_A^2 \int_{-\eta_0}^{\eta_0} \tau_i d\eta \cosh \eta \epsilon(\tau_i, \eta) \approx \int_{p_T > p_0, |y| < \eta_0} d^3p E \frac{d\sigma^{NN}}{d^3p} \cdot T_{AA}(0). \quad (32)$$

Here the first part is a general relation for a flow $\Theta = \eta$; the second part shows where it is computed from. Due to the boost factor $\cosh \eta$, which in the jet computation corresponds to the weight factor E , most of the energy is carried by flow at large rapidities. When η_0 approaches the beam rapidity y_{beam} , the error in the jet computation grows for two reasons: firstly, baryon number will be important at large rapidities and secondly, physics there is not that of independent $2 \rightarrow 2$ collisions. However, this error is important only at very large values of η , where the energy density is already small. It thus will not affect the conclusions of this hydrodynamical study.

4 Analytic approximations

We are studying modifications to the Bjorken flow and it is appropriate to ask whether they in some limit can be described analytically. Consider the limit $\sigma \gg 1$, a broad gaussian (31). Writing ($\hat{t} = \log(\tau/\tau_i)$)

$$\epsilon(\tau, \eta) = \epsilon_0 \exp\left\{-\frac{4}{3}\hat{t} - \frac{\eta^2}{2\sigma^2} + g(\tau)\right\}, \quad (33)$$

$$\Theta(\tau, \eta) = \eta[1 + f(\tau)], \quad (34)$$

linearising eqs.(11-12) under the assumptions $f, g, \eta^2/\sigma^2 \ll 1$ and integrating, one obtains

$$f(\tau) = \frac{3}{8\sigma^2}[1 - \exp(-\frac{2}{3}\hat{t})], \quad (35)$$

$$g(\tau) = -\frac{1}{2\sigma^2}\left\{\hat{t} - \frac{3}{2}[1 - \exp(-\frac{2}{3}\hat{t})]\right\}. \quad (36)$$

The linearisation $\partial_i f \gg f^2$ demands that

$$\hat{t} \ll 3 \log\left(\frac{4}{3}\sigma\right). \quad (37)$$

Furthermore, for the flow lines one obtains

$$\log[\eta^{\text{flow}}(\tau)/\eta_0] = \frac{3}{8\sigma^2}\left\{\hat{t} - \frac{3}{2}[1 - \exp(-\frac{2}{3}\hat{t})]\right\} \quad (38)$$

These equations contain the following natural expectations:

- The energy density at $\eta \approx 0$ decreases faster than in the Bjorken flow due to energy moving to larger η . For small times

$$\epsilon(\tau) = \epsilon_0 \exp\left[-\frac{4}{3}\left(\hat{t} + \frac{\hat{t}^2}{8\sigma^2} + \dots\right)\right]; \quad (39)$$

- With increasing time the flow is accelerated relative to the similarity flow. For small times

$$\Theta(\tau, \eta) = \eta\left(1 + \frac{\hat{t}}{4\sigma^2} + \dots\right); \quad (40)$$

- The flow lines bend outwards. For small times

$$\eta^{\text{flow}}(\tau) = \eta_0\left(1 + \frac{\hat{t}^2}{8\sigma^2} + \dots\right). \quad (41)$$

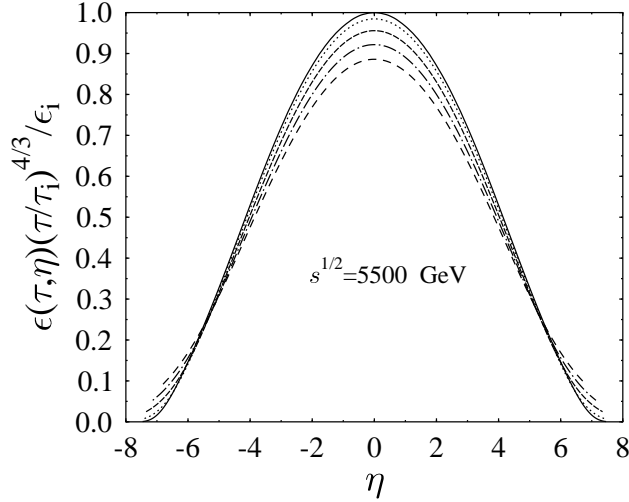


Figure 3: The energy density scaled by the Bjorken flow, $\epsilon(\tau, \eta)/\epsilon_i * (\tau/\tau_i)^{4/3}$, for $\sqrt{s} = 5500$ GeV. From top the curves correspond to $\tau/\tau_i = 1, 10^{1/2}, 10, 10^{3/2}, 100$.

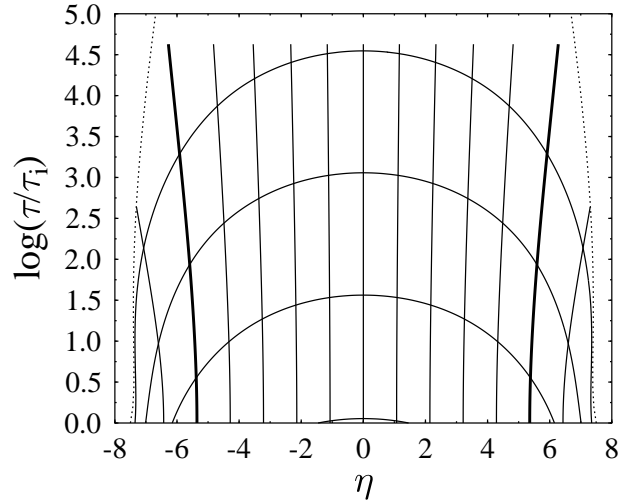


Figure 4: Curves of constant $\epsilon(\tau, \eta)$ for $\sqrt{s} = 5500$ GeV. The curves from below at $\eta = 0$ correspond to $\epsilon = 900, 117, 15, 2$ GeV/fm³. The vertical lines are flow lines ($\eta = \text{constant}$ for Bjorken flow). The thick flow lines are used to compute fig. 6. The dotted lines are the leftmost characteristic curve C^+ and the rightmost C^- , between which the computation has to remain.

5 Numerical results

The method of characteristics [16] is particularly suited for 1+1 dimensional hydrodynamical problems. First the differential equation [14]

$$\frac{d\eta}{dt} = \tanh[\Theta(\hat{t}, \eta) - \eta \pm y_s], \quad (42)$$

where $y_s = \tanh c_s = \tanh(1/\sqrt{3})$, defines the two families C^\pm of characteristics. This is like the equation (15) defining the flowlines, but modified by the sound rapidity $\pm y_s$. Along each family of curves the changes of Θ and ϵ are related by

$$d\Theta \pm \frac{c_s}{\epsilon + p} = 0, \quad \text{along } C^\pm. \quad (43)$$

A code integrating ϵ, Θ , starting from the initial values $\epsilon(\tau_i, \eta), \Theta(\tau_i, \eta) = \eta$ by determining the characteristic directions, and then the new values of ϵ, Θ by stepping in the characteristic directions, is easily constructed.

Results of numerical integration of the equations are shown in Figs. 3-6 for LHC ($\sqrt{s} = 5500$ GeV). The energy density, scaled by the Bjorken flow, is shown in fig. 3 as a function of η at different times. Curves of constant energy density on the τ, η plane are plotted in fig. 4. The energy density in fig. 3 at $\eta = 0$ is seen to decrease somewhat faster than in the Bjorken case. This is due to leakage of energy to larger rapidities, seen as an increase in ϵ at large η and described analytically in section 4. During the whole duration of the plasma phase, $\epsilon \gtrsim 2$ GeV/fm³, or from τ_i to about $100\tau_i$, this additional decrease is about 12% at LHC.

Converted to the lifetime of the system in the plasma phase (the time it takes to decrease from ϵ_i to ϵ_c) the above result implies that the density gradient in the longitudinal direction decreases the lifetime by about 9%. This is opposite to the effects of dissipation: in the case of a rapidity plateau, the fastest decrease of energy density is obtained in the case of full thermalisation; dissipative effects increase the lifetime of the system [10]. The longest lifetime is obtained for free-streaming expansion.

Fig. 4 also shows flow lines, which are constant in η in the Bjorken case but bend outwards in the present case. We do not show the numerical grid of characteristic curves, but the leftmost characteristic curve C^+ and the rightmost one C^- are plotted in this figure. The numerical computation cannot be extended outside them.

The flow $\Theta(\tau, \eta)$, scaled by the Bjorken flow η , is shown in fig. 5. The initial flow $\Theta = \eta$ is rapidly accelerated at large $|\eta|$, due to increasing $\partial_\eta p/p$, ($=\eta/\sigma^2$ for the gaussian parametrization) but this is already in the domain where the details of the model need not be correct. In the relevant region near $\eta = 0$ the effects are seen to be small, a few %.

As discussed earlier, the total entropy between two flow lines, eq.(17), is constant. However, the flow rapidity $\Theta(\tau, \eta)$ changes along the flow lines changing also the rapidity interval between the flow lines. As a result the entropy of given fluid element is shifted in rapidity and its amount per unit flow rapidity is changed. With our initial conditions the shift is always to larger rapidities — higher pressure in the central region accelerates the fluid towards the ends — and the rapidity intervals between the flow lines increase. The net result is that the entropy per unit flow rapidity, which can be expressed as

$$\frac{dS(\tau, \eta)}{d\Theta} = \pi R_A^2 \tau s(\tau, \eta) \cosh[\Theta(\tau, \eta) - \eta] \frac{d\eta}{d\Theta} \Big|_{\text{fixed } \tau}, \quad (44)$$

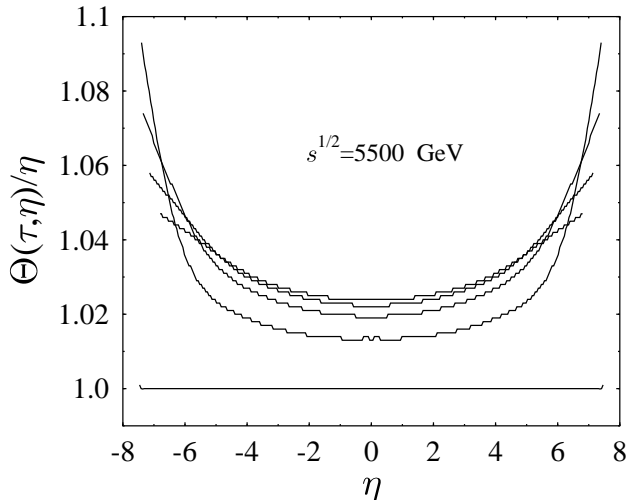


Figure 5: The flow rapidity scaled by η , $\Theta(\tau, \eta)/\eta$, for $\sqrt{s} = 5500$ GeV. The curves at $\eta = 0$ correspond from below to values of τ as in fig. 3.

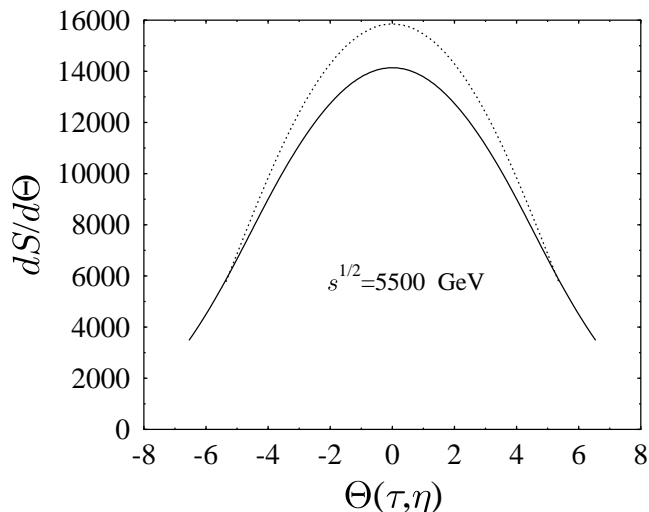


Figure 6: The total entropy per unit Θ between the two thick flow lines in fig. 4 for $\sqrt{s} = 5500$ GeV. The dotted curve corresponds to $\tau = \tau_i$ and the solid one to $\tau = 100\tau_i$.

will decrease in the central region and the overall distribution will get wider.

The result of our computation for $dS/d\Theta$ is shown in Fig. 6. In η the computation is extended between the two (arbitrarily chosen) thick flow lines in Fig. 4. The dotted curve shows the initial distribution at $\tau_i = 0.1$ fm and the solid curve the final distribution at $\tau = 100\tau_i$. Note that the end points move outwards due to a combination of two effects: the flow lines bend outwards (Fig. 4) and the flow is accelerated relative to η (Fig. 5).

To obtain a measurable distribution we should be able to treat the hadronization and to fold the thermal motion of final particles with the collective motion of the flow

(after expressing the entropy in terms of particle number densities). At present, we do not have a reliable way to estimate the effects of hadronization but if it has any effects on flow we would expect them to further widen the rapidity distribution as the hadronization proceeds from the lower density fragmentation regions to the central region. Thermal folding involves flow velocities effectively over two-to-three rapidity units. It will lead to a somewhat wider overall rapidity distribution but in the smooth central region the effect of folding is small. We conclude that our result of Fig. 6 gives the minimum change from the initial state at τ_i to the rapidity distribution of final particles.

6 Conclusions

In the case of a fully developed rapidity plateau, there is a very simple hydrodynamical scaling solution for the longitudinal expansion of QCD matter produced in ultrarelativistic heavy ion collisions [1]. In reality, there need not be a rapidity plateau, and we have studied the longitudinal flow using a rapidity distribution of the initial energy density obtained from computations in perturbative QCD. Then the rapidity distribution is approximately gaussian but very broad, and thus the deviations from the Bjorken flow are not very large. To analyze the general features of the flow we also derived equations for the total entropy and energy between two flow lines and gave approximate solutions in the limit of broad gaussians for the central region.

The finite width of the rapidity region leads to a transfer of energy from the central region to larger rapidities. As a consequence the rapidity distribution gets wider and the energy density in the central region decays faster than for a boost invariant flow. Correspondingly, the lifetime of the system (the time it takes to decrease from ϵ_i to ϵ_c) decreases by about 10%. A similar decrease would be caused by transverse density gradients. On the other hand, dissipative effects would increase the lifetime.

The longitudinal density gradient also leads to some but very small acceleration of the longitudinal flow: the effect in the central region is rather on the 1% than 10% level. In the sense our results confirm the assumptions in [9], called the frozen motion model in [12], that in estimating thermal effects in the central region it is reasonable to assume that at LHC energies the longitudinal flow velocity scales even when the density distributions are not boost invariant.

References

- [1] J. Bjorken, Phys. Rev. D27 (1983) 140.
- [2] J.-P. Blaizot and A. Mueller, Nucl. Phys. B289 (1987) 847.
- [3] K. J. Eskola, K. Kajantie and J. Lindfors, Nucl. Phys. B323 (1989) 37.

- [4] K. J. Eskola, K. Kajantie and P. V. Ruuskanen, Phys. Lett. B332 (1994) 191 [hep-ph/9404237].
- [5] K. Kajantie and K. J. Eskola, nucl-th/9610015, Zeitschrift für Physik C, in print.
- [6] H1 Collaboration, S. Aid et al., Nucl. Phys. B470 (1996) 3, C. Adloff et al., hep-ex/9703012; ZEUS Collaboration, M. Derrick et al., Z. Phys. C72 (1996) 399.
- [7] P. V. Ruuskanen, Acta Physica Polonica B16 (1997) 551.
- [8] D. Rischke, S. Bernard and J. Maruhn, Nucl. Phys. A595 (1995) 346; D. Rischke, Y. Pürsün and J. Maruhn, Nucl. Phys. A595 (1995) 383; D. Rischke, Nucl. Phys. A610 (1996) 88c.
- [9] R. Vogt, B. V. Jacak, P. L. McGaughey, and P. V. Ruuskanen, Phys. Rev. D49 (1994) 3345 [hep-ph/9309213].
- [10] K. J. Eskola and M. Gyulassy, Phys. Rev. C47 (1993) 2329.
- [11] J. Sollfrank, P. Huovinen, M. Kataja, P. V. Ruuskanen, M. Prakash and R. Venugopalan, Phys. Rev. C55 (1997) 392 [nucl-th/9607029].
- [12] E. V. Shuryak and L. Xiong, Phys. Lett. B333 (1994) 316.
- [13] M. Gyulassy, D. Rischke and Bin Zhang, Nucl. Phys. A613 (1997) 397 [nucl-th/9609030].
- [14] K. Kajantie, R. Raitio and P. V. Ruuskanen, Nucl. Phys. B222 (1983) 152.
- [15] E. Laermann, Proc. Quark Matter '96, Nucl. Phys. A610 (1996) 1c.
- [16] L. Collatz, Numerical treatment of differential equations, Springer Verlag, Heidelberg, 1959, p. 318.